



Computer-generated global map of valley networks on Mars

Wei Luo¹ and T. F. Stepinski²

Received 3 February 2009; revised 21 July 2009; accepted 4 August 2009; published 20 November 2009.

[1] The presence of valley networks (VN) on Mars suggests that early Mars was warmer and wetter than present. However, detailed geomorphic analyses of individual networks have not led to a consensus regarding their origin. An additional line of evidence can be provided by the global pattern of dissection on Mars, but the currently available global map of VN, compiled from Viking images, is incomplete and outdated. We created an updated map of VN by using a computer algorithm that parses topographic data and recognizes valleys by their morphologic signature. This computer-generated map was visually inspected and edited to produce the final updated map of VN. The new map shows an increase in total VN length by a factor of 2.3. A global map of dissection density, D , derived from the new VN map, shows that the most highly dissected region forms a belt located between the equator and mid-southern latitudes. The most prominent regions of high values of D are the northern Terra Cimmeria and the Margaritifer Terra where D reaches the value of 0.12 km^{-1} over extended areas. The average value of D is 0.062 km^{-1} , only 2.6 times lower than the terrestrial value of D as measured in the same fashion. These relatively high values of dissection density over extensive regions of the planet point toward precipitation-fed runoff erosion as the primary mechanism of valley formation. Assuming a warm and wet early Mars, peculiarity of the global pattern of dissection is interpreted in the terms of climate controlling factors influenced by the topographic dichotomy.

Citation: Luo, W., and T. F. Stepinski (2009), Computer-generated global map of valley networks on Mars, *J. Geophys. Res.*, *114*, E11010, doi:10.1029/2009JE003357.

1. Introduction

[2] Martian valley networks (hereafter referred to as VN), discovered in 1971 by the Mariner 9 spacecraft, are geomorphic features on Mars exhibiting some visual resemblance to terrestrial river systems. The VN are present mostly in the Martian highlands and date mostly to the Noachian [Fassett *et al.*, 2008; Hoke and Hynes, 2008]. They point to a possibility that Noachian Mars was warmer and wetter than present-day Mars, perhaps capable of maintaining precipitation and some form of life. A geomorphic analysis of VN should, in principle, be able to establish a predominant style of erosion leading to their formation. Finding features indicative of runoff erosion signals precipitation and a warmer climate whereas features indicative of erosion by groundwater sapping allow for cold and dry conditions during the formation of VN. Alas, the geomorphic evidence is inconclusive and the origin of VN remains a topic of active research.

[3] The VN are not as mature and integrated as typical terrestrial analogues. Many VN exhibit widely spaced tributaries with alcove-like terminations [Sharp and Malin, 1975; Pieri, 1980], constant valley width downstream [Goldspiel *et al.*, 1993], short, stubby tributaries [Baker

and Partridge, 1986], flat longitudinal profiles [Aharonson *et al.*, 2002], and U-shaped cross sections [Carr, 1995]. On Earth such features are attributed to erosion by groundwater sapping. Groundwater sapping, which rarely dominates on Earth, generates landforms quite different from landforms formed by rainfall-fed runoff erosion [Laiy and Malin, 1985; Howard, 1988; Luo *et al.*, 1997]. The formation of VN by sapping could happen in cold and dry conditions, providing that groundwater was recharged by some mechanism such as hydrothermal circulation [Gulick and Baker, 1990; Tanaka *et al.*, 1998].

[4] On the other hand, runoff origin of VN is supported by branching, dendritic patterns, origin near dividing ridges [Milton, 1973; Irwin and Howard, 2002; Craddock and Howard, 2002; Hynes and Phillips, 2003; Stepinski and Collier, 2004], consistency with crater degradation [Craddock and Maxwell, 1993; Craddock *et al.*, 1997; Forsberg-Taylor *et al.*, 2004], and significant erosion [Goldspiel and Squyres, 1991; Grant, 2000; Gulick, 2001]. In addition, surface runoff is necessary to carry away the debris generated by potential groundwater sapping [Craddock and Howard, 2002; Lamb *et al.*, 2006]. Runoff origin of VN points to precipitation on early Mars.

[5] A common feature of all aforementioned studies is their reliance on detailed examination of selected valley segments or individual networks. However, these detailed studies must be supplemented by an analysis of an overall dissection pattern in order to formulate a viable hypothesis of VN origin. Pattern analysis requires a global, sufficiently

¹Department of Geography, Northern Illinois University, DeKalb, Illinois, USA.

²Lunar and Planetary Institute, Houston, Texas, USA.

detailed map of VN. The existing global map was drawn by Carr [Carr, 1995; Carr and Chuang, 1997] using Viking-based images covering $\pm 65^\circ$ of latitude. The Carr map contains $\sim 348,000$ km of valleys; taken globally it depicts an immature drainage heavily concentrated in the southern highlands. The newer, different types of global mosaics of Mars, such as the Mars Orbiter Laser Altimeter (MOLA) Mission Experiment Gridded Data Records (MEGDR) [Smith et al., 2003], or THEMIS mosaic [Christiansen, 2004] reveal existence of many valleys not depicted in Carr's map [Hynek and Phillips, 2003; Mangold et al., 2004; Stepinski and Collier, 2004; Ansan and Mangold, 2006]. Therefore, construction of a new, more comprehensive global map of VN is in order. The absence of such map is due to the high cost of its acquisitions by standard means of visual interpretation of images, although there is an effort underway [Hynek et al., 2008] to construct such a map.

[6] Recent advances in machine extraction of geomorphic features from topographic data [Molloy and Stepinski, 2007] make it feasible to acquire the VN map automatically - by computer parsing of the MEGDR. In this paper we use such automated approach to construct a planet-wide map of VN that would reveal more accurately the global pattern of dissection on Mars. The resultant map shows much more dense dissection than was depicted by [Carr and Chuang, 1997]. This result adds to the growing body of evidence that points toward precipitation-fed runoff erosion as an ultimate origin of VN, and thus toward the warm and wet climate on early Mars. We propose to explain the different patterns of dissection on early Mars and Earth in terms of different global topographies of the two planets rather than in terms of the overall availability of liquid water.

[7] The rest of the paper is organized as follows: section 2 describes methodology and results of mapping the valley networks. Section 3 discusses the methodology for deriving a global map of dissection density from the mapped VN and zonal statistics of the dissection density. Finally, in section 4 we discuss our results, assess the utility of the new maps, and point to directions of future development.

2. Mapping Valley Networks

2.1. Mapping Methodology

[8] In principle, the THEMIS daytime IR data set of images represents the best quality global representation of the Martian surface, but lack of reliable autodetection methods of VN from images prevents its utilization for our purposes. On the other hand, topographic data provide more direct information on landscape dissection and a suitable input for automapping of VN. The Martian global topographic data set (digital elevation model or DEM) is available as the MEGDR [Smith et al., 2003]. We use the MEGDR DEM with spatial resolution of 128 pixels/degree or about 463 m/pixel at the equator. Note that MEGDR is an interpolated DEM, as the cross-track spacing of the original MOLA measurements is variable and ~ 1000 m at the equator [Neumann et al., 2001] so some of the grid cells lack actual measurement values. This limitation on the quality of the available data means that some valleys or portions of the valleys, located in places where the MEGDR is smudged due to lack of data, may not be properly mapped by our algorithm.

[9] The core technology underpinning our mapping method has been developed by Molloy and Stepinski [2007]. It detects incisions directly from terrain morphology, making it possible to accurately map regions with highly variable drainage density. The valleys are mapped only where they are "seen" by an algorithm without resorting to any particular model of dissection. The emphasis on mapping rather than modeling the location of VN is what distinguishes our method from previous applications of computer algorithms to delineate the VN. Modeling the drainage network from a DEM by assuming a uniform and constant rainfall and a particular criterion for surface channelization is routinely performed in terrestrial hydrology [O'Callaghan and Mark, 1984; Tarboton et al., 1991, 1992; Montgomery and Dietrich, 1992; Peckham, 1995]. These modeling methods were also applied to individual VN on Mars [Stepinski et al., 2002, 2004; Caldarelli et al., 2004; Mest and Crown, 2008] in order to compare manually mapped networks with model predictions. However, the model-based automatic delineation of drainage fails to provide an accurate global map of VN because the underlying assumptions of the model, while apt to terrestrial conditions, are apparently unsuitable for Mars.

[10] The basic idea behind our method is to flag landforms having a U-shaped morphology that is characteristic of the valleys. Using terrain morphology to extract valleys and drainage networks had been proposed in the past [Peucker and Douglas, 1975; Band, 1986; Howard, 1994; Tarboton and Ames, 2001], however, these early attempts had not led to robust mapping algorithms as they were unable to overcome a key technical challenge of minimizing the noise in calculation of a terrain parameter used to flag the valleys. The algorithm developed by Molloy and Stepinski [2007] calculates the topographic planar curvature (TPC) analytically for each pixel in the DEM using a polynomial approximation to the local patch of the surface. This method minimizes noise in the values of the TPC. The TPC influences the divergence/convergence of potential flow. The positive values of the TPC flag segments of terrain where flow converges (we refer to them as U-shaped terrain), whereas the negative values of the TPC flag segments of terrain where flow diverges. Thus, the valleys are identified as segments with relatively large positive values of the TPC ($TPC > 0.003 \text{ m}^{-1}$ has been used in the present calculations). Note that TPC is a local measure, so valleys wider than ~ 10 pixels (~ 5 km) may not register as U-shaped features. Molloy and Stepinski [2007] have designed a number of image processing transformations that turn these segments into an actual map of VN.

[11] Details of the accuracy assessment of the automapping algorithm were given by Molloy and Stepinski [2007]. Here we briefly summarize the result from that study. The accuracy was assessed based on eight test sites having areas on the order of 10^5 km^2 each. For these sites manual delineations of VN (based on the THEMIS daytime IR images with the resolution of 100 m/pixel) were compared with the results of automapping using quantitative measures pertaining to the overall length of the valleys, size of the watershed, and the physical "closeness" of the two networks. Overall, they found a good agreement between manual and automatic mapping. The total length of auto-mapped valleys is less than the total length of drawn

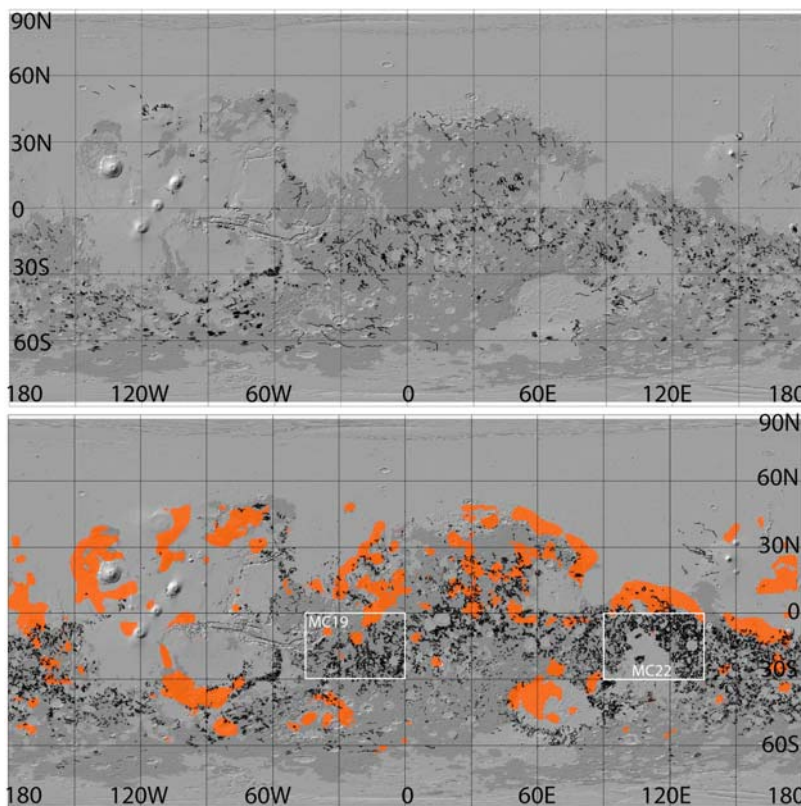


Figure 1. Visual comparison of valley networks mapping: (top) the Carr map and (bottom) the map generated by our algorithm. Dark gray background indicates extent of the Noachian terrain. Regions where the algorithm has identified large number of false valleys are shown in orange. Two quadrangles previously mapped using our algorithm are outlined in white.

valleys; however this difference is attributed to the different resolutions of THEMIS and MEGDR data sets. The watersheds of automapped VN are larger than the watersheds of drawn VN because automapped networks benefit from topographic information and conform better to the underlying landscape. Finally, the automapped and drawn networks are “close” to each other as measured by a statistics of differences between pixel-to-valley drainage lengths calculated using the two networks.

[12] The automapping algorithm has also been tested for mapping VN over the entire quadrangles. Application of this algorithm to the Mare Tyrrenum (MC22) quadrangle [Luo and Stepinski, 2006], yielded 172,396 km of U-shaped features, of which 142,885 km were visually confirmed to be actual VN. For comparison, only 25,447 km of VN are present in the Carr map of this quadrangle. Similarly, applying our algorithm to the Margaritifer Sinus (MC19) quadrangle [Stepinski *et al.*, 2007] yielded 115,429 km of VN versus 33,949 km of VN present in the Carr map of the same region. The locations of these quadrangles are indicated in Figure 1.

[13] We have set to automap the VN located between 50°N and 70°S on Mars. In order to obtain a global map we subdivided the entire MEGDR into overlapping tiles having a size of 10° by 10° each. This mosaicing is necessitated by the size of the complete MEGDR-based DEM (46080 × 22528 pixels) that is too large to be processed in its entirety. The overlapping buffer (with a width of 100 km) between adjacent tiles prevents mapping incomplete valley frag-

ments. The valleys are identified and measured at each tile separately and the results from individual tiles are concatenated into a single database from which duplicate valleys, which are present due to buffering, are eliminated before the final map is created.

2.2. Mapping Results

[14] The resulting (unverified) map was placed into an ArcGIS shapefile that contained ~375,550 individual valley segments. A segment is an unbifurcated line on a map; it corresponds to a single “link” [Rodriguez-Iturbe and Rinaldo, 1997] in a drainage network. For comparison, the Carr map contains 11,336 segments. In order to facilitate future analyses a database of actual networks instead of segments is more desirable. A network is a set of connected segments organized in a hierarchical system starting from the outlet and bifurcating in the upstream direction. In order to create a database of VN we parsed the set of 375,550 individual segments to determine which segments are associated with each other and thus can be combined into a network. The result of this calculation is another ArcGIS shapefile, visually identical to the original shapefile of segments, but containing 178,012 “netlets.” Due to the limited quality of the topographic data and the degraded character of many VN our parsing algorithm is unable to collect all segments constituting a complete network (as interpreted by an analyst). The best it can do is to group segments that connect to each other. We refer to these agglomerates as netlets. Depending on the state of preservation of a given

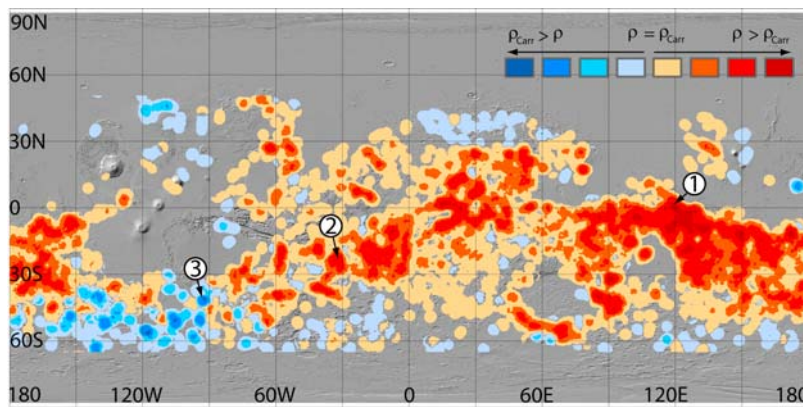


Figure 2. Quantitative comparison of valley networks mapping using the difference, $\rho - \rho_{\text{Carr}}$, of line densities calculated for each map. Areas chosen for in-depth comparison are labeled 1 to 3.

VN and the quality of the MEGDR in its location, it may take anywhere from a single netlet to several netlets to represent an actual network. The database of netlets (an attribute table associated with the netlets shapefile) lists numerical attributes associated with each netlet: ID number, outlet coordinates, location (bounding box), the underlying geologic units, the number of segments in the netlet, netlets's order and magnitude [Rodriguez-Iturbe and Rinaldo, 1997], total length of all tributaries in the netlet, the length of the main valley, the elevation of the outlet and source of the main valley, sinuosity, slope and aspect of the main valley, and the area of a drainage basin associated with the netlet.

[15] Visual inspection of the uncorrected map of netlets reveals that our automapping procedure yields a lot of false positives (objects that are not really valleys), especially outside of the Noachian surface. This is expected because the algorithm identifies all features having a U-shaped morphology. In the Noachian a great majority of such features are indeed valleys, but other features on Mars surface, such as, for example, grabens, also may be recognized as having a U-shaped morphology. In order to eliminate false negatives we visually inspected and edited the original, unverified map. The result is a corrected map containing 24,941 netlets. Thus, 86% of netlets are eliminated by visual inspection, many of which are small single segment netlets resulting from imperfection in the data. Eliminated netlets (false positives) constitute 76% of the total length of the features originally mapped as “valleys.” On Figure 1 (bottom) we indicated the regions on Mars where the algorithm has mapped a large number of false positives. These include areas located along the dichotomy boundary, around the Olympus Mons, Tharsis bulge, Alba Patera, at the floors of big impact craters such as Hellas and Argyre, all characterized by tectonic and/or volcanic activities. The total length of the valleys in the corrected database is 807,000 km, approximately 2.3 times the total length of valleys in the Carr map. Figure 1 shows a visual comparison between the Carr map and our automapped, corrected map. Our algorithm finds VN in the same regions (mostly Noachian) where they have been mapped by Carr, but it finds more of them.

[16] Figure 1 offers only a qualitative comparison between the two maps. In order to perform a quantitative comparison we calculated the line density, ρ , of valleys as

shown on the two maps. Line density at a given location is the density of linear features (valleys) in the neighborhood of that location, i.e., the total length of valleys divided by the area of the neighborhood. We have used a grid of sampling locations with 4 km spacing. For each location, a circle centered on that location and having a radius of 150 km was used as a neighborhood. The result of the line density calculation is a raster where each pixel has a value of ρ calculated on the basis of its neighborhood. As applied to VN, the concept of line density is very similar to the concept of drainage density. However, whereas drainage density pertains to hydrology, the line density pertains to graphics. In calculating ρ the neighborhood over which lines are accumulated is chosen arbitrarily and its shape and size are fixed throughout the region. In calculating drainage density the neighborhood is a drainage basin, its shape and size are dictated by the topography and changes throughout the region. Thus, values of ρ cannot serve as estimates of drainage density and we utilize them only for assessing the difference between the two maps.

[17] Figure 2 shows a map of $\rho - \rho_{\text{Carr}}$. The regions shown in warm colors (yellow-to-brown) are the areas where our corrected map depicts more valleys (by length) than the Carr map. The regions shown in cool colors (light blue-to-dark blue) are the areas where Carr map depicts more valleys. The new map depicts more valleys almost everywhere. The most notable exceptions are Aonia Terra and Terra Sirenum located at high southern latitudes, and Alba Patera and the northernmost extent of Arabia Terra located in the mid northern latitude. We have chosen three specific close-up sites, annotated 1, 2, and 3 on Figure 2, to demonstrate the differences between the two maps. The first two sites demonstrate locations where our algorithm has mapped significantly more valleys than are present in the Carr map. The third site focuses on a location where our algorithm extracted less valleys than are present in the Carr map.

[18] Site 1 (Figure 3) is located in the Terra Cimmeria and centered on 121.21°E and 1.22°N; the background image is the THEMIS daytime IR mosaic. The Carr map (Figure 3b) registers a single prominent network and another less prominent channel. Note that the Carr map is not correctly registered with the MDIM 2.1 standard resulting in a misalignment between the map of the network and the

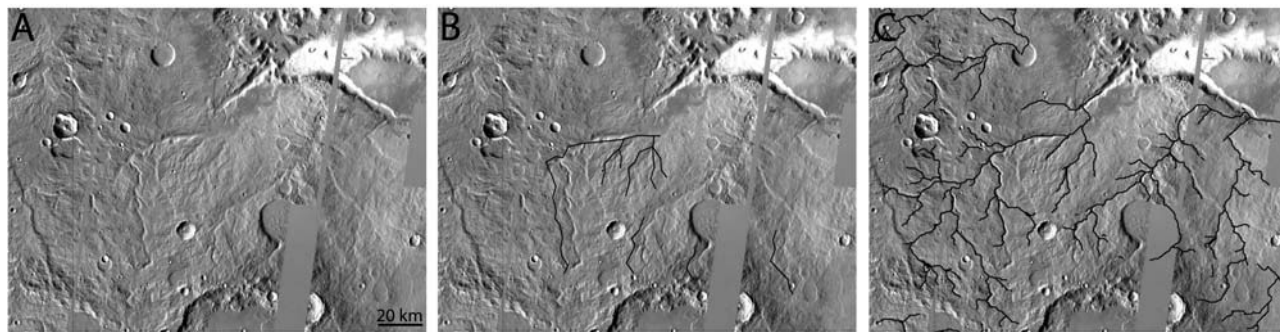


Figure 3. Close-up of the VN mapping in a site labeled 1 in Figure 2. The site is located in the Terra Cimmeria and centered on 121.21°E and 1.22°N. (a) Image of the site, (b) Carr map of VN, and (c) the autogenerated map of VN. The background image is the THEMIS daytime IR mosaic.

image. Our map (Figure 3c) registers 5.8 more valleys (by length) in the same site than the Carr map does. Site 2 (Figure 4) is located on the southwestern flank of the Ladon basin and centered on 32.22°W and 20.41°S; the site includes the Arda Valles. The Carr map (Figure 4b) shows the Arda Valles, but it does not show an extensive system of valleys located to the east and southeast of the Arda Valles which is clearly visible in the THEMIS image. Again, our autogenerated map (Figure 4c) registers most valleys seen in the THEMIS image, 2.6 times more (by length) than are present on the Carr map.

[19] Finally, Site 3 (Figure 5) is centered on 92.41°W and 41.84°S and shows the Warrego Valles: arguably the best known example of VN on Mars. Figures 5a and 5b show THEMIS daytime IR image and shaded relief derived from the MEGDR, respectively. Also shown in Figure 5b are MOLA tracks. Although the network is clearly visible in the image, it is much less prominent in the topography as depicted by the MEGDR. As it happens the quality of the MEGDR in the location of the Warrego Valles is rather poor; MOLA tracks show gaps several kilometers wide in some places (Figure 5b). The lack of data results in a presence of many smudges obscuring the network. Consequently, the Carr map (Figure 5c) registers 2.3 times more valleys (by length) than our algorithm does (Figure 5d). Moreover, during the process of manual editing, we have apparently overcorrected the original automap (Figure 5d) resulting in further reduction of channels (Figure 5e). The

Warrego Valles site represents a rare example of location where our autogenerated map shows less valleys than the Carr map. Such sites are associated with the locations where MEGDR quality is below average. There is also a possibility that we have inadvertently deleted some actual valleys during the manual edit of an uncorrected automap.

3. Mapping Dissection Density

3.1. Methodology

[20] The map of VN depicts the spatial distribution of dissection on Mars and provides a convenient tool for visual and descriptive analysis of the dissection pattern. However, the map of VN is not well suited for a quantitative analysis geared toward determining factors responsible for the observed pattern of dissection. In order to utilize the information contained in the map of VN for quantitative, computer-based analyses we derive a raster map of dissection density. Dissection density, D , is conventionally defined as the total length of valleys per unit area. When the area is well defined, for example, a geological unit or drainage basin, calculation of D from a map of VN is straightforward. However, often such spatial units are not readily available. Moreover, even when the spatial units are defined, conventional calculation does not facilitate mapping variations in D within each individual, possibly much extended, unit. These problems are addressed by utilizing a generalized measure of D that is defined for every pixel in a



Figure 4. Close-up of the VN mapping in the Arda Valles site labeled 2 in Figure 2. The Arda Valles site is centered on 32.22°W and 21.41°S. (a) Image of the site, (b) Carr map of VN, and (c) the autogenerated map of VN. The background image is the THEMIS daytime IR mosaic.

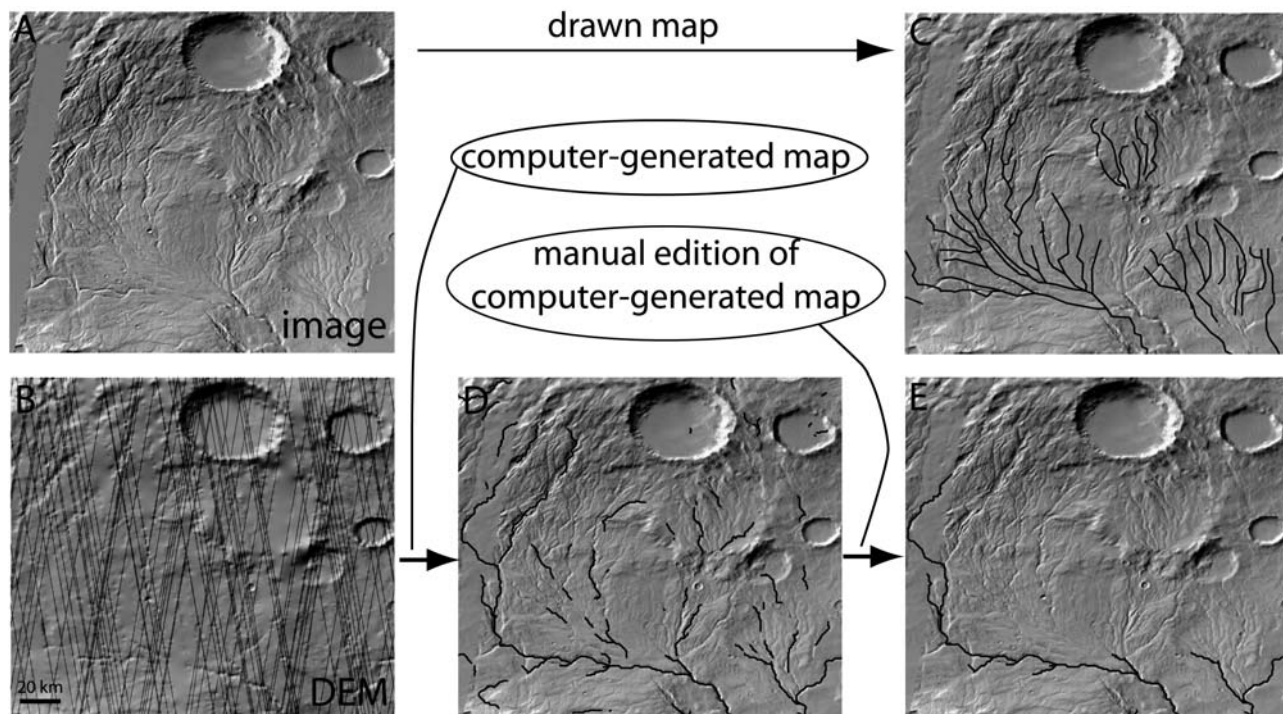


Figure 5. Close-up of the VN mapping in the Warrego Valles site labeled 3 in Figure 2. The Warrego Valles site is centered on 92.41°W and 41.84°S . (a) THEMIS daytime IR mosaic image of the site, (b) shaded relief based on the MEGDR, along with MOLA tracks, (c) Carr map of VN, (d) uncorrected, autogenerated map of VN, and (e) corrected, autogenerated map of VN.

DEM and does not require predefined spatial units for its calculation. We refer to such measure as the “continuous” dissection density.

[21] The continuous dissection density is defined [Tucker et al., 2001] in terms of a local (pixel-based) and easily calculated variable, $L(x, y)$: the downslope distance to the nearest valley from a given pixel (x, y) . The mean value $\langle L \rangle$, calculated over a specified neighborhood of (x, y) is physically related to dissection density at the point (x, y) .

$$D(x, y) = \frac{1}{2\langle L \rangle} \quad (1)$$

[22] We use a correlation length of $L(x, y)$, Λ , as the size of the neighborhood over which the average $\langle L \rangle$ is calculated. Λ , read from the covariance function of $L(x, y)$, is the distance beyond which L is not autocorrelated. This allows for calculating the value of D for every pixel in the DEM, for which a drainage path to a channel exists, resulting in construction of a continuous raster map of dissection density. Note there is a difference between the continuous dissection density and the line density used in section 2.2. Although both measures are pixel-based, D utilizes local topography and the estimated size of an average drainage basin (Λ), while ρ ignores topography and is based on an arbitrary length scale. Thus, whereas the values of D are reasonable estimates of actual drainage density, the values of ρ are not. In section 2.2 we were forced to use ρ because the valleys, as depicted on the Carr map, do not conform to topography so calculating D from the Carr map is not possible.

3.2. Results

[23] We used the MEGDR together with the corrected automap of VN to calculate $L(x, y)$. The $D(x, y)$ raster was calculated using a correlation length of about 150 pixels. Figure 6 shows the map of $D(x, y)$, the blue-to-red gradient depicts values of $D(x, y)$ from its minimum of 0.00014 km^{-1} to its maximum of 1.08 km^{-1} . The effective range of D values is $0-0.12 \text{ km}^{-1}$, the few values larger than 0.12 km^{-1} are outliers caused by computational artifacts. The mean value of D is 0.062 km^{-1} and the value of standard deviation is 0.041 km^{-1} . The areas not covered by the color gradient are places where D is not defined. Comparing the map of D (Figure 6) with the map of VN (Figure 1, bottom), it is clear that the two maps convey the same information about the spatial distribution of dissection, but the map of D does it more effectively by readily identifying locations with different levels of dissection.

[24] According to the map on Figure 6 the distribution of D is rather homogeneous on large spatial scale; the dissected region forms a belt roughly located between the equator and mid southern latitudes. At the same time the distribution of D is quite inhomogeneous on smaller spatial scales; although the mean value of D is high throughout the aforementioned belt, there is a strong local variability. The most prominent region of concentrated areas of high dissection density is located in the northern Terra Cimmeria, around and northwest of the Herschel Crater and extending up to the dichotomy boundary. Another region of high dissection density is located in the Margaritifer Terra. These two regions are located in quadrangles MC22 and MC19; these are the quadrangles that we automapped for VN [Luo

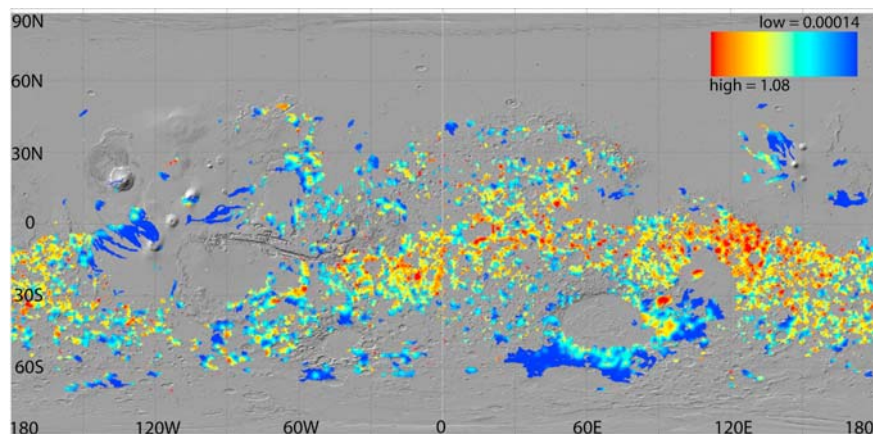


Figure 6. Global map of dissection density, D , on Mars. The blue-to-red gradient corresponds to low-to-high values of D , and gray indicates areas for which D is undefined.

and Stepinski, 2006; Stepinski *et al.*, 2007] before attempting to generate a global map.

3.3. Statistical Analysis

[25] We take advantage of the fact that $D(x, y)$ is a raster of the same dimensions as the MEGDR and calculate zonal statistics of dissection density with respect to several variables. The zonal statistics is a tool that allows us to calculate statistics (such as the mean, standard deviation etc.) of D for a number of predefined spatial zones. A zone is a set of pixels having a common attribute.

[26] First, we calculate zonal statistics of D with respect to latitude. The latitudes covered by our map (50°N to 70°S) are classified into 12 equidistant zones. For each zone the values of mean and standard deviation of D are calculated using only pixels located with this zone. The result of this calculation is shown on Figure 7a. The zonal statistics of D with respect to latitude encapsulates what is already seen on the map of D (Figure 6); regions located between the equator and $\sim 40^{\circ}\text{S}$ have on average the highest density of dissection.

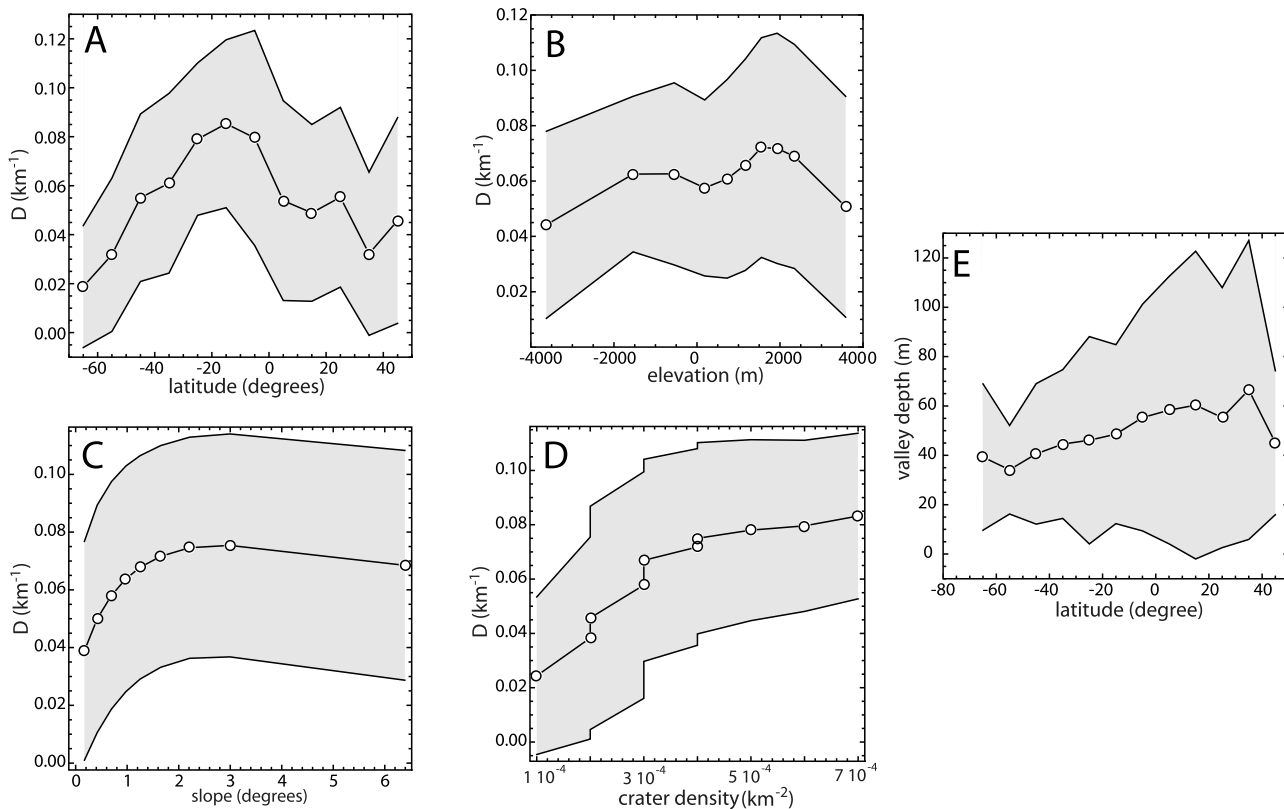


Figure 7. Zonal statistics of dissection density D with respect to (a) latitude, (b) elevation, (c) slope, and (d) crater density. (e) Zonal statistics of valley depths with respect to latitude. Circles indicate mean values for each zone. The regions spanning the values of average \pm standard deviation are shown in gray.

[27] Second, we calculate zonal statistics of D with respect to elevation. To derive elevation zones we use only the MEGDR pixels for which D is defined (only pixels represented by a color in Figure 6). These pixels are classified into 10 zones in such a fashion that each zone contains approximately the same number of pixels (equal area classification). The result of zonal statistics of D with respect to elevation is shown on Figure 7b. It shows that, on average, the highest dissection density occurs in the regions located at elevations between 1000 m and 3000 m; these range of elevations coincides with the prominent belt of high values of D clearly seen on Figure 6 with a notable exception of the Margaritifer Terra which is located at lower elevations corresponding to a secondary hump in Figure 7b. Similarly, we have calculated zonal statistics of D with respect to the local slope (Figure 7c). The steepest-descent-based slope values are calculated from the MEGDR only at the pixels for which D is defined. These pixels are classified into 9 zones using an equal area classification. The result of zonal statistics of D with respect to slope is shown on Figure 7c; on average, steeper locations are more dissected.

[28] Finally, we calculate zonal statistics of D with respect to crater density. The crater density is derived from the Catalog of Large Martian Impact Craters [Barlow, 1988] using a circular moving window with a radius of 150 km. A given pixel is assigned a value of crater density corresponding to a ratio of the total count of craters in a circular window to the area of the window. The pixels for which D is defined are classified into 10 zones using an equal area classification. Figure 7d shows the results of zonal statistics of D with respect to crater density; it shows that dissection density and crater density are positively correlated.

[29] In addition, we have calculated zonal statistics of estimated valley depths with respect to latitude. The valley depths are estimated from DEM using a procedure described in [Howard et al., 2005] and [Barnhart et al., 2009]. Elevation values are collected from within a 3 km radius of a focus pixel identified as belonging to a valley. The 75th percentile elevation is assumed to capture the elevation of the surrounding surface; valley depth is estimated as a difference between the elevation of the surrounding surface and the elevation at the focus pixel. This procedure is repeated for all pixels delineating VN. Figure 7e shows that, on average, the valleys are shallowest in the southernmost locations and their depth systematically increases northward.

4. Discussion

[30] We demonstrated that semiautomapping of VN on a global scale is a feasible technique that offers speed and objectivity. Using our mapping technique we produced a significant update to Carr's global map of VN. All products associated with our map, uncorrected segments, uncorrected netlets, and corrected netlets, as well as the global map of continuous dissection density are available from the authors upon request.

4.1. Interpretation of Mapping Results

[31] Our map shows that the dissection is most prominent in a wave-like region (see Figure 6) located in the Noachian surface and extending roughly from the equator to mid southern latitudes. The crest of this "wave" is located at

60°E to 120°E, and the trough of the "wave" is located at 90°W to 150°W. The northern limit of the region of intensive dissection is mostly controlled by the geology; it approximately coincides with the northern extent of the Noachian surface. However, the southern limit of the high dissection region cannot be explained by the global geology and constitutes the first major feature of the global distribution of D that needs explanation. The large scale of the global map (Figure 6) makes it difficult to observe spatial distribution of D on smaller length scales. Zooming into the smaller spatial scales reveals a patchy character of dissection; local highs, where the values of D are as high as 0.12 km^{-1} , are interweaved with local lows, where the values of D are much lower or the surface lacks dissection altogether. This patchy distribution of D cannot be attributed exclusively to covering by subsequent processes, and appears to be a salient characteristic of an original emplacement of valleys; it constitutes the second major feature of the global distribution of D that requires explanation.

[32] These two major features of the global distribution of dissection were already noticeable in the Carr map; the major new insight from our updated global map of VN is the value of dissection density that is higher than was reported by Carr. [Carr and Chuang, 1997] found dissection density on Mars (as measured on $\sim 1 \text{ km}$ length scale) to be an order of magnitude lower than on Earth. The disparity of the values of D on the two planets provided a major argument against runoff erosion as the leading mechanism of the VN formation. However, the mean value of D , as calculated from our map, is 0.062 km^{-1} . Our preliminary calculation for Earth using the same methodology and topographic data of similar resolution yielded a mean value of D for terrestrial landmass of 0.16 km^{-1} or only 2.6 times higher than on Mars. By using topographic data instead of images, and by resorting to a (semi)automatic mapping technique, we were able to map significantly more valleys thus reducing the disparity between the values of dissection density (as measured on $\sim 1 \text{ km}$ length scale) on the two planets. (It is important to recall that terrestrial values of D , as measured on $\sim 30 \text{ m}$ length scale are $1\text{--}100 \text{ km}^{-1}$ [Knighton, 1998]; however, small valleys are not expected to survive on Mars, so dissection densities on the two planets need to be compared on a larger spatial scale.) Given the relatively high values of D over the large portion of Noachian surface, it is now difficult to argue against runoff erosion as the major mechanism of VN formation. This conclusion, arrived on the basis of examining the global pattern of dissection, supplements similar conclusions arrived on the basis of detailed examinations of individual valleys (see section 1).

[33] The zonal statistics (see section 3.3) provides few clues into the origin of VN. Zonal statistics of D with respect to latitude and elevation basically points to the geographical location of VN. The zonal statistics of D with respect to the local slope shows increased dissection of steeper terrain, a feature consistent with runoff erosion processes [Montgomery and Dietrich, 1989]. Statistics of D with respect to crater density points to potential correlation between cratering and dissection. However, it is more likely that crater density serves as yet another proxy for the geographical location of the highly dissected region and less likely that it indicates any direct casual relation between cratering and dissection. The region of high crater density on Mars [Stepinski and

Urbach, 2009] has many of the same geographical limits as the region of intensive dissection. Finally, the zonal statistics of valley depth with respect to latitude shows shallowing toward the south pole. Thus, not only the number of valleys decreases drastically southward of $\sim 30\text{--}40^\circ\text{S}$, but their depths decrease as well. This is in agreement with the results of similar calculations by [Williams and Phillips, 2001]. This trend could be a primordial feature related to the mechanism of valleys emplacement (see discussion below), the effect of subsequent surface modification, or the combination of both. Indeed, the terrain located southward of $\sim 30\text{--}40^\circ\text{S}$ is known for its “softened” appearance. This attribute of mid-to-high-latitude terrain is connected to surface modification due to either mantling [Soderblom *et al.*, 1973] or viscous relaxation due to presence of ground ice [Parmentier and Head, 1981]. Terrain softening may result in postformation shallowing of valleys located southward of $\sim 30\text{--}40^\circ\text{S}$.

[34] The full account of implications the global pattern of dissection has on the origin of VN is beyond the scope of this paper. However, we offer a preliminary discussion of a particular scenario that may, conceivably, explain the major features of this pattern. This scenario is based on an exploratory discussion of climatic controlling factors on ancient Mars [Richardson and Soto, 2008]. We focus on explaining why the pattern of dissection on Mars is different from the terrestrial pattern, even assuming a best case scenario of an early Mars that was warm enough to support liquid water on its surface. The fundamental reason is the existence of the topographic dichotomy on Mars. Given the particular global topography of Mars, the water will accumulate in the topographic lows of the northern plains to form an “ocean.” The confinement of a major water reservoir to northern plains restricts the transfer of water vapor to equatorial regions and the southern hemisphere where the VN are found. Global atmospheric circulation will carry moisture from northern midlatitudes southward resulting in precipitation when the air mass rises orographically upon encountering the dichotomy boundary. In fact, some of the heavily dissected regions are found where the topographic dichotomy is the most pronounced (see Figure 6). The supply of moisture to the regions located farther from the ocean would be limited. Diffusive atmospheric motions will deliver occasional storms to these regions, but in quantities much smaller than could be expected from the global inventory of water. Thus, in this scenario the equatorial and southern regions of Mars would experience an arid, “continental” climate not because of the lack of liquid water on the surface of the planet, but because of the physical separation of the water reservoir and the landmass. Such a scenario explains the relatively low dissection density and the existence of the southern limit to the presence of valley networks. The southernmost regions, located farthest from the water reservoir would get no rainfall and would develop no valleys. It also offers an explanation to shallowing of VN from (roughly) the location of topographic dichotomy, where largest rainfall rates result in more dissection, southward, where smaller rainfall rates result in less dissection. This hypothesis requires further scrutiny; in particular, it needs to be investigated whether potential existence of large “lakes” in the Hellas and Argyre basins would alter our reasoning. It is unclear how to

explain the patchy character of dissection within a framework of this scenario.

4.2. Automapping Technique: Issues and Future Research

[35] Mapping any features by means of computer parsing of digital data is a challenging problem because even the best algorithm lacks human comprehension of the problem and is unable to make a determination on the basis of a broader context. Our algorithm, in its present form, cannot distinguish between valleys and other landscape features having a U-shaped morphology. It is also not designed to extrapolate the valleys (as a human mapper would frequently do) to the parts of the landscape where topographic data is of inferior quality or lacking altogether. In this paper the first shortcoming is solved by means of visual inspection of the initial, uncorrected map produced by the algorithm. Thus, strictly speaking our mapping technique is semiautomated because the final map of valley networks requires verification from additional imagery data. Although such a semi-automatic technique is faster and more objective than purely manual mapping, the ultimate goal is to develop a fully automatic technique of mapping VN. Our future research will focus on the development of an algorithm, based on a concept of machine learning [Witten and Frank, 2005], that can automatically eliminate false positives. In machine learning the features that are known a priori to be VN are used to “train” an algorithm and to build a mathematical model of a valley network against which all “candidate networks” are tested for either inclusion or elimination. This would allow us to do away with manual editing. The second shortcoming is not addressed in this paper; the valleys are mapped where they are “seen” (by the algorithm) in the data and no attempt is made to extrapolate the netlets so they form more integrated networks. Although models of drainage can be used for such extrapolation (see discussion in section 1) it is prudent to deliver a model-free map and to leave the modeling to the user of the map in cases it is deemed helpful or necessary.

[36] Is it “cost effective” to develop a technique for automapping of VN? The up-front cost of developing an automapping algorithm is high but this expense is recuperated by a low operating cost of actual mapping. On the other hand, manual mapping requires little up-front investment but it imposes large operating cost. Because there is no evidence that valleys extend to ever smaller spatial scales, we don’t expect automapping of VN to offer the same “economy of scale” advantage as, for example, the automapping of craters which can be used to map “millions” of small craters. Nevertheless, we submit that developing a means for autoanalysis of planetary data is an important task because, in general, purely manual analysis is not efficient enough for analyzing the deluge of new data. Our effort to automap VN develops techniques that can be used for mapping other landscape features, too. In addition, automapped VN, while sometimes lacking the integration of manually mapped VN, possess some other characteristics that are absent from manual maps. For example, automapped VN are guaranteed to conform fully to topography, whereas manually mapped VN are not. Automapping is also an objective and reproducible procedure. Finally, the method developed for automapping VN can be applied [Luo and

Stepinski, 2008] to map the drainage on Earth where automation can be used to map even the smallest valleys. This provides a new functionality for terrestrial geomorphology because conventional methods for mapping dissection are model-based and fail in the regions where model assumptions are not fulfilled, like, for example, in regions where dissection density changes abruptly [Luo and Stepinski, 2008].

[37] **Acknowledgments.** We acknowledge support by NASA (W.L. under grant NNX08AM98G, T.F.S. under grant NNG05GM316). A portion of this research was conducted at the Lunar and Planetary Institute under contract CAN-NCC5-679 with NASA. This is LPI contribution 1503. We would like to thank Robert Craddock and an anonymous reviewer for their thorough reviews. Yi Qi and Bartosz Grudzinski helped with the manual editing of VN.

References

- Aharonson, O., M. T. Zuber, D. H. Rothman, and K. X. Whipple (2002), Drainage basins and channel incision on Mars, *Proc. Natl. Acad. Sci.*, *99*, 1780–1783.
- Ansan, V., and N. Mangold (2006), New observations of Warrego Valles, Mars: Evidence for precipitation and surface runoff, *Planet. Space Sci.*, *54*(3), 219–242.
- Baker, V. R., and J. B. Partridge (1986), Small Martian valleys: Pristine and degraded morphology, *J. Geophys. Res.*, *91*, 3561–3572.
- Band, L. B. (1986), Topographic partition of watersheds with digital elevation models, *Water Resour. Res.*, *22*(1), 15–24.
- Barlow, N. G. (1988), Crater size-distributions and a revised Martian relative chronology, *Icarus*, *75*(2), 285–305.
- Barnhart, C. J., A. D. Howard, and J. M. Moore (2009), Long-term precipitation and late-stage valley network formation: Landform simulations of Parana Basin, Mars, *J. Geophys. Res.*, *114*, E01003, doi:10.1029/2008JE003122.
- Caldarelli, G., P. D. L. Rios, M. Montuori, and V. D. P. Servedio (2004), Statistical features of drainage basins in Mars channel networks, *Eur. Phys. J. B*, *38*(2), 387–391.
- Carr, M. H. (1995), The Martian drainage system and the origin of valley networks and fretted channels, *J. Geophys. Res.*, *100*, 7479–7507.
- Carr, M. H., and F. C. Chuang (1997), Martian drainage densities, *J. Geophys. Res.*, *102*, 9145–9152.
- Christiansen, P. R. (2004), Themis public data release, technical report, PDS Node, Ariz. State Univ., Mesa, Ariz. (Available at <http://themis.asu.edu>)
- Craddock, R. A., and A. D. Howard (2002), The case for rainfall on a warm, wet early Mars, *J. Geophys. Res.*, *107*(E11), 5111, doi:10.1029/2001JE001505.
- Craddock, R. A., and T. Maxwell (1993), Geomorphic evolution of Martian highlands through ancient fluvial process, *J. Geophys. Res.*, *98*, 4353–4368.
- Craddock, R. A., T. A. Maxwell, and A. D. Howard (1997), Crater morphology and modification in the Sinus Sabaeus and Margaritifer Sinus regions of Mars, *J. Geophys. Res.*, *102*, 13,321–13,340.
- Fassett, C. I., J. W. Head, and J. L. Dickson (2008), Mars valley networks: Chronology and environments, in *Second Workshop on Mars Valley Networks*, pp. 20–24, Smithsonian Inst., Washington, D. C.
- Forsberg-Taylor, N. K., A. D. Howard, and R. A. Craddock (2004), Crater degradation in the Martian highlands: Morphometric analysis of the Sinus Sabaeus region and simulation modeling suggest fluvial processes, *J. Geophys. Res.*, *109*, E05002, doi:10.1029/2004JE002242.
- Goldspiel, J. M., and S. W. Squyres (1991), Ancient aqueous sedimentation on Mars, *Icarus*, *105*(2), 479–500.
- Goldspiel, J. M., S. W. Squyres, and D. G. Jankowski (1993), Topography of small Martian valleys, *Icarus*, *105*(2), 479–500.
- Grant, J. A. (2000), Valley formation in Margaritifer Sinus, Mars, by precipitation-recharged groundwater sapping, *Geology*, *28*(3), 223–226.
- Gulick, V. C. (2001), Origin of the valley networks on Mars: A hydrological perspective, *Geomorphology*, *37*, 241–268.
- Gulick, V. C., and V. R. Baker (1990), Origin and evolution of valleys on Martian volcanoes, *J. Geophys. Res.*, *95*, 14,325–14,344.
- Hoke, M. R. T., and B. M. Hynek (2008), Roaming zones of precipitation on ancient Mars recorded in valley networks, in *Second Workshop on Mars Valley Networks*, pp. 31–34, Smithsonian Inst., Washington, D. C.
- Howard, A. D. (1988), Introduction: Groundwater sapping on Mars and Earth, in *Sapping Features of the Colorado Plateau*, *NASA Spec. Publ.* *491*, pp. 1–5, NASA, Washington, D. C.
- Howard, A. D. (1994), A detachment-limited model of drainage basin evolution, *Water Resour. Res.*, *30*(7), 2261–2286.
- Howard, A. D., J. M. Moore, and R. P. Irwin (2005), An intense terminal epoch of widespread fluvial activity on early Mars: 1. Valley network incision and associated deposits, *J. Geophys. Res.*, *110*, E12S14, doi:10.1029/2005JE002459.
- Hynek, B. M., and R. J. Phillips (2003), New data reveal mature, integrated drainage systems on Mars indicative of past precipitation, *Geology*, *31*(9), 757–760.
- Hynek, B. M., M. Beach, and M. R. T. Hoke (2008), Updated global map of Martian valley networks: Implications for hydrologic processes, in *Second Workshop on Mars Valley Networks*, pp. 39–42, Smithsonian Inst., Washington, D. C.
- Irwin, R. P., and A. D. Howard (2002), Drainage basin evolution in Noachian Terra Cimmeria, Mars, *J. Geophys. Res.*, *107*(E7), 5056, doi:10.1029/2001JE001818.
- Knighton, D. (1998), *Fluvial Forms and Processes: A New Perspective*, Edward Arnold, London.
- Laity, J. B., and M. C. Malin (1985), Sapping processes and the development of theater-headed valley networks in the Colorado Plateau, *Geol. Soc. Am. Bull.*, *96*, 203–217.
- Lamb, M. P., A. D. Howard, J. Johnson, K. Whipple, W. B. Dietrich, and J. T. Perron (2006), Can springs cut canyons into rock?, *J. Geophys. Res.*, *111*, E07002, doi:10.1029/2005JE002663.
- Luo, W., and T. F. Stepinski (2006), Topographically derived maps of valley networks and drainage density in Mare Tyrrhenum quadrangle on Mars, *Geophys. Res. Lett.*, *33*, L18202, doi:10.1029/2006GL027346.
- Luo, W., and T. Stepinski (2008), Identification of geologic contrast from landscape dissection pattern: An application to the Cascade Range, Oregon, USA, *Geomorphology*, *99*, 90–98.
- Luo, W., M. K. Crombie, N. Sturchio, Z. E. Alf, R. E. Arvidson, M. Sultan, and R. Becker (1997), Groundwater sapping process, Western Desert, Egypt, *Geol. Soc. Am. Bull.*, *109*, 43–62.
- Mangold, N., C. Quantin, V. Ansan, C. Delacourt, and P. Allemand (2004), Evidence for precipitation on Mars from dendritic valleys in the Valles Marineris area, *Science*, *305*, 78–81.
- Mest, S. C., and D. A. Crown (2008), Comparison of mapped and modeled watersheds in the Tyrrhena Terra region of Mars, in *Second Workshop on Mars Valley Networks*, pp. 55–58, Smithsonian Inst., Washington, D. C.
- Milton, D. J. (1973), Water and processes of degradation in the Martian landscape, *J. Geophys. Res.*, *78*, 4037–4047.
- Molloy, I., and T. F. Stepinski (2007), Automatic mapping of valley networks on Mars, *Comput. Geosci.*, *33*(6), 728–738.
- Montgomery, D., and W. Dietrich (1989), Source areas, drainage density, and channel initiation, *Water Resour. Res.*, *25*, 1907–1918.
- Montgomery, D. R., and W. E. Dietrich (1992), Channel initiation and the problem of landscape scale, *Science*, *255*, 826–830.
- Neumann, G. A., D. D. Rowlands, F. G. Lemoine, D. E. Smith, and M. T. Zuber (2001), Crossover analysis of Mars Orbiter Laser Altimeter data, *J. Geophys. Res.*, *106*, 23,753–23,768.
- O’Callaghan, J. F., and D. M. Mark (1984), The extraction of drainage networks from digital elevation data, *Comput. Vision Graph. Image Proc.*, *28*(3), 323–344.
- Parmentier, E., and J. Head (1981), Viscous relaxation of impact craters on icy planetary surfaces: Determination of viscosity variation with depth, *Icarus*, *47*, 100–111.
- Peckham, S. D. (1995), Self-similarity in the three-dimensional geometry and dynamics of large river basins, Ph.D. thesis, Univ. of Colo., Boulder.
- Peucker, T. K., and D. H. Douglas (1975), Detection of surface-specific points by local parallel processing of discrete terrain elevation data, *Comput. Graph. Image Proc.*, *4*, 375–387.
- Pieri, D. C. (1980), Martian valleys: morphology, distribution, age, and origin, *Science*, *210*, 895–897.
- Richardson, M. I., and A. Soto (2008), Controls on precipitation and aridity for ancient Mars, in *Second Workshop on Mars Valley Networks*, pp. 62–65, Smithsonian Inst., Washington, D. C.
- Rodriguez-Iturbe, I., and A. Rinaldo (1997), *Fractal River Basins, Chance and Self-Organization*, Cambridge Univ. Press, Cambridge, U. K.
- Sharp, R. P., and M. C. Malin (1975), Channels on Mars, *Geol. Soc. Am. Bull.*, *86*, 593–609.
- Smith, D., G. Neumann, R. E. Arvidson, E. A. Guinness, and S. Slavney (2003), Mars Global Surveyor laser altimeter mission experiment gridded data record, technical report, NASA Planet. Data Syst., NASA, Washington, D. C.
- Soderblom, L., T. Kreidler, and H. Masursky (1973), Latitudinal distribution of a debris mantle on the Martian surface, *J. Geophys. Res.*, *78*, 4117–4122.
- Stepinski, T. F., and M. L. Collier (2004), Extraction of Martian valley networks from digital topography, *J. Geophys. Res.*, *109*, E11005, doi:10.1029/2004JE002269.

- Stepinski, T. F., M. M. Marinova, P. J. McGovern, and S. M. Clifford (2002), Fractal analysis of drainage basins on Mars, *Geophys. Res. Lett.*, 29(8), 1189, doi:10.1029/2002GL014666.
- Stepinski, T. F., M. L. Collier, P. J. McGovern, and S. M. Clifford (2004), Martian geomorphology from fractal analysis of drainage networks, *J. Geophys. Res.*, 109, E02005, doi:10.1029/2003JE002098.
- Stepinski, T. F., W. Luo, and Y. Qi (2007), Precision mapping of valley networks in Margaritifer Sinus, Mars, *Proc. Lunar Planet. Sci. Conf.*, 38th, Abstract 1205.
- Stepinski, T. F., and E. R. Urbach (2009), The first automatic survey of impact craters on Mars: Global maps of depth/diameter ratio, *Proc. Lunar Planet. Sci. Conf.*, 40th, Abstract 1117.
- Tanaka, K. L., J. Dohm, J. Lias, and T. M. Hara (1998), Erosional valleys in the Thaumasia region of Mars: Hydrothermal and seismic origins, *J. Geophys. Res.*, 103, 31,407–31,419.
- Tarboton, D. G., and D. P. Ames (2001), Advances in the mapping of flow networks from digital elevation data, in *World Water and Environmental Resources Congress*, ASCE, Orlando, Fla.
- Tarboton, D. G., R. L. Bras, and I. Rodriguez-Iturbe (1991), On the extraction of channel networks from digital elevation data, *Hydrol. Proc.*, 5, 81–100.
- Tarboton, D. G., R. L. Bras, and I. Rodriguez-Iturbe (1992), A physical basis for drainage density, *Geomorphology*, 5, 59–76.
- Tucker, G. E., F. Catani, A. Rinaldo, and R. L. Bras (2001), Statistical analysis of drainage density from digital terrain data, *Geomorphology*, 36, 187–202.
- Williams, R. M. E., and R. J. Phillips (2001), Morphometric measurements of Martian valley networks from Mars Orbiter Laser Altimeter (MOLA) data, *J. Geophys. Res.*, 106, 23,737–23,751.
- Witten, I. H., and E. Frank (2005), *Data Mining: Practical Machine Learning Tools and Techniques, Second Edition (Morgan Kaufmann Series in Data Management Systems)*, Morgan Kaufmann Publ., San Francisco, Calif.

W. Luo, Department of Geography, Northern Illinois University, DeKalb, IL 60115, USA. (wluo@niu.edu)

T. F. Stepinski, Lunar and Planetary Institute, 3600 Bay Area Blvd., Houston, TX 77058, USA. (tom@lpi.usra.edu)